7th European Workshop on Structural Health Monitoring
July 8-11, 2014. La Cité, Nantes, France

MODE SELECTIVE ACTUATOR-SENSOR SYSTEM FOR LAMB WAVE-BASED STRUCTURAL HEALTH MONITORING

Daniel Schmidt[1], Peter Wierach[1], Michael Sinapius[2]

[1] *German Aerospace Center (DLR e. V.), Institute of Composite Structures and Adaptive Systems, Lilienthalplatz 7, 38108 Braunschweig, Germany*
[2] *Technische Universität Braunschweig, Institute of Adaptronics and Functional Integration, Langer Kamp 6, 38106 Braunschweig, Germany*

daniel.schmidt@dlr.de

ABSTRACT

Structural Health Monitoring (SHM) based on Lamb waves, a type of ultrasonic guided waves, is a promising method for in-service inspection of composite structures. In this study mode selective actuators and sensors are investigated to excite a particular Lamb wave mode in composite plates. The actuator and sensor exhibit an interdigital transducer design. In order to describe the complex displacement fields of A_0 and S_0 mode and to characterize the mode selectivity of the transducers a two dimensional analytical model based on higher order laminated plate theory is developed.

KEYWORDS : *Structural health monitoring, Lamb waves, higher order plate theory, actuator-sensor system, CFRP plates.*

INTRODUCTION

Structural Health Monitoring (SHM) based on Lamb waves, a type of ultrasonic guided waves, is a promising technique for in-service inspection of composite structures. However, the presence of at least two Lamb wave modes (symmetric modes, S_0, S_1, S_2,…, and anti-symmetric modes, A_0, A_1, A_2,…) at any given frequency, their dispersive characteristic and their interference at structural discontinuities produce complex wave propagation fields and sensor signals which are difficult to evaluate. In order to reduce the complexity of the wave propagation field mode selective actuator-sensor systems are investigated. These actuator-sensor systems are able to generate and receive a particular Lamb wave mode in CFRP plates (carbon fibre-reinforced plastic).
In the present study a two dimensional analytical model using higher order laminated plate theory is developed. The plate theory is based on second and third order displacement functions to approximate the complex displacement fields of A_0 and S_0 mode. The plate theory is solved under the boundary conditions of an actuator in order to obtain the strain distribution of the Lamb wave propagation field. On the sensor side the strain distribution is converted into electrical voltage using the constitutive relations of piezoelectric material. The actuator and sensor exhibit an interdigital transducer design. With this type of transducer a particular Lamb wave mode can be amplified because the frequency as well as the wavelength can be controlled. With the analytical model different configurations of the transducers are analysed with respect to the amplitude ratio of A_0 and S_0 mode.

1 ANALYTICAL MODEL

In order to amplify a specific Lamb wave mode and to simultaneously attenuate the other modes an actuator sensor configuration based on interdigital transducer design is used. As proposed in [1], [2], [3], interdigital transducers are a promising mode selective method. With these transducers it is possible to control the frequency as well as the wavelength of the desired mode within the excitation in order to amplify a particular Lamb wave mode. The electrode configuration is made of two comb-like electrodes with opposite polarity. The electrode distance corresponds to the half-

wavelength of the desired Lamb wave mode which will be excited at a frequency in the plate structure. The aim of the analytical model is to evaluate the amplitudes of S_0 and A_0 mode between actuator sensor configurations in CFRP plates. With the model the mode selective characteristics can be estimated and optimized. The main effects, that influence the amplitudes of Lamb waves as well as the mode selectivity, are summarized in the following:

- Dispersion and attenuation in the plate structure
- Design and configuration of transducers
- Shear-lag between transducers and structure
- Resonances of the transducers
- Excitation signal and frequency filter

All these effects, apart from the transducer resonances, are considered in the model to calculate realistic amplitudes of Lamb waves. The following Figure 1 shows the components as well as the setup of the model. The interdigital transducers are modelled as individual segments, which exhibit piezoelectric properties.

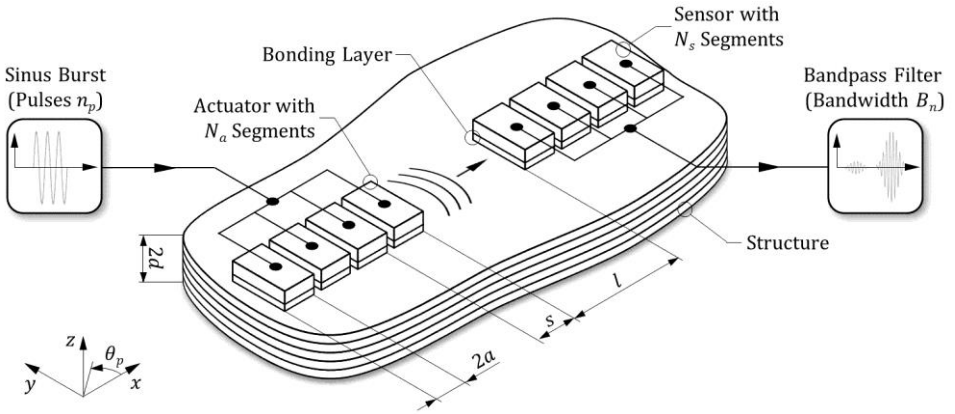

Figure 1 : Components of the actuator sensor configuration based on interdigital transducers

The amplitudes of S_0 and A_0 mode are calculated using higher order laminated plate theory. For Lamb wave applications the higher order plate theory is typically utilized to determine the dispersion and attenuation in composite plates [4], [5], [6]. In the present study the higher order plate theory is solved under the boundary condition of an actuator excitation to evaluate the strain distribution in the plate structure. Therefore the equation of motion can be derived from the Lagrange equation:

$$\frac{d}{dt}\frac{\partial \mathcal{L}}{\partial \dot{\boldsymbol{u}}} - \frac{\partial \mathcal{L}}{\partial \boldsymbol{u}} = \tilde{\boldsymbol{\sigma}}, \qquad \mathcal{L} = T - V \tag{1}$$

where $\tilde{\boldsymbol{\sigma}}$ are the mechanical stresses on the upper surface of the plate structure:

$$\tilde{\boldsymbol{\sigma}} = \left(\tilde{\tau}_{xz} \;\; \tilde{\tau}_{yz} \;\; \tilde{\sigma}_z \;\; d\,\tilde{\tau}_{xz} \;\; d\,\tilde{\tau}_{yz} \;\; d\,\tilde{\sigma}_z \;\; d^2\tilde{\tau}_{xz} \;\; d^2\tilde{\tau}_{yz} \;\; d^2\tilde{\sigma}_z \;\; d^3\tilde{\tau}_{xz} \;\; d^3\tilde{\tau}_{yz}\right)^T \tag{2}$$

The kinetic T and strain energy V are given by:

$$\begin{aligned} T &= \frac{1}{2}\dot{\boldsymbol{u}}^T \rho \dot{\boldsymbol{u}}\,, \qquad \boldsymbol{u} = [u \;\; v \;\; w]^T \\ V &= \frac{1}{2}\boldsymbol{\varepsilon}^T \boldsymbol{C}\boldsymbol{\varepsilon}\,, \qquad \boldsymbol{\varepsilon} = [\varepsilon_x \;\; \varepsilon_y \;\; \varepsilon_z \;\; \varepsilon_{yz} \;\; \varepsilon_{xz} \;\; \varepsilon_{xy}]^T \end{aligned} \tag{3}$$

In order to describe attenuation effects of the plate structure the stiffness matrix C_{ij} of each CFRP layer is assumed to be a complex quantity. The real part relates to the elastic and the imaginary part to the viscous behaviour [5]:

$$C_{ij} = C_{ij}^{Re} + iC_{ij}^{Im}, \qquad C_{ij}^{Im} = \eta_{ij} \tag{4}$$

For the viscous behaviour the hysteretic model, where the viscosity coefficients η_{ij} are independent from frequency is assumed. As shown in [7], the attenuation of Lamb waves in CFRP plates can be well approximated with the hysteretic model. The displacement $\boldsymbol{u}$ and strain field $\boldsymbol{\varepsilon}$ can be determined with the following higher order functions [6]:

$$u = u_0(x,y,t) + z\,\psi_x(x,y,t) + z^2\phi_x(x,y,t) + z^3\chi_x(x,y,t) \tag{5}$$

$$v = v_0(x,y,t) + z\,\psi_y(x,y,t) + z^2\phi_y(x,y,t) + z^3\chi_y(x,y,t) \tag{6}$$

$$w = w_0(x,y,t) + z\,\psi_z(x,y,t) + z^2\phi_z(x,y,t) \tag{7}$$

With these second and third order functions the S_0 and A_0 mode can be approximated over large frequency range. Considering harmonic solutions with respect to time and x-y direction, the assumption for the displacement field is in the form:

$$\boldsymbol{u}_0 = \hat{\boldsymbol{u}}_0 e^{i(k_x x + k_y y - \omega t)}, \qquad \begin{aligned} \boldsymbol{u}_0 &= [u_0 \;\; v_0 \;\; w_0 \;\; \psi_x \;\; \psi_y \;\; \psi_z \;\; \phi_x \;\; \phi_y \;\; \phi_z \;\; \chi_x \;\; \chi_y]^T \\ \hat{\boldsymbol{u}}_0 &= \left[\hat{u}_0 \;\; \hat{v}_0 \;\; \hat{w}_0 \;\; \hat{\psi}_x \;\; \hat{\psi}_y \;\; \hat{\psi}_z \;\; \hat{\phi}_x \;\; \hat{\phi}_y \;\; \hat{\phi}_z \;\; \hat{\chi}_x \;\; \hat{\chi}_y\right]^T \end{aligned} \tag{8}$$

where $k_x = k\cdot\cos(\theta_p)$ and $k_y = k\cdot\sin(\theta_p)$ are complex wavenumbers in x-y direction. After the implementation of the displacement fields given by equation (8) into (3) and solving the Lagrange equation (1) the equation of motion for Lamb wave propagation are obtained in the form:

$$\hat{\boldsymbol{u}}_0(k,\omega) = \boldsymbol{L}^{-1}\tilde{\boldsymbol{\sigma}}, \qquad \tilde{\boldsymbol{\sigma}} = (\tilde{\tau}_{xz} \;\; 0 \;\; d\,\tilde{\tau}_{xz} \;\; 0 \;\; d^2\tilde{\tau}_{xz} \;\; 0 \;\; d^3\tilde{\tau}_{xz})^T \tag{9}$$

The formulation of the mechanical stresses $\tilde{\boldsymbol{\sigma}}$ implicate, that the actuator produces only shear stresses on the upper surface of the plate and the model is reduced into a two-dimensional problem. In case of symmetric CFRP laminates the equation of motion can be derived into two independent solutions (left: symmetric modes, right: anti-symmetric modes):

$$\begin{bmatrix}\hat{u}_0\\ \hat{\psi}_z\\ \hat{\phi}_x\end{bmatrix} = \begin{bmatrix}L_{11}^S & L_{13}^S & L_{14}^S\\ L_{13}^S & L_{33}^S & L_{34}^S\\ L_{14}^S & L_{34}^S & L_{44}^S\end{bmatrix}^{-1}\begin{bmatrix}\tilde{\tau}_{xz}\\ 0\\ d^2\tilde{\tau}_{xz}\end{bmatrix}, \qquad \begin{bmatrix}\hat{w}_0\\ \hat{\psi}_x\\ \hat{\phi}_z\\ \hat{\chi}_x\end{bmatrix} = \begin{bmatrix}L_{11}^A & L_{12}^A & L_{14}^A & L_{15}^A\\ L_{12}^A & L_{22}^A & L_{24}^A & L_{25}^A\\ L_{14}^A & L_{24}^A & L_{44}^A & L_{45}^A\\ L_{15}^A & L_{25}^A & L_{45}^A & L_{55}^A\end{bmatrix}^{-1}\begin{bmatrix}0\\ d\,\tilde{\tau}_{xz}\\ 0\\ d^3\tilde{\tau}_{xz}\end{bmatrix} \tag{10}$$

The coefficients L_{ij} are given in the Appendix. The inverse matrix $\boldsymbol{L}^{-1}$ can be expressed in form of its adjoint $\boldsymbol{N}$ and determinant $\boldsymbol{D}$. Applying the inverse Fourier transformation the solution can be converted into the spartial domain:

$$\hat{\boldsymbol{u}}_0(x,\omega) = \frac{1}{2\pi}\int_{-\infty}^{\infty}\frac{\boldsymbol{N}(k)}{D(k)}\tilde{\boldsymbol{\sigma}}e^{ikx}\,dk \tag{11}$$

The integral can be calculated by Cauchy's theorem of residues, as presented in [8]:

$$\oint_C f(k)\,\mathrm{d}k = 2\pi i\sum_k Res[f(k)], \;\; \mathrm{Res}[f(k)] = \frac{\mathrm{N}(k)}{D'(k)} \tag{12}$$

where D' represents the derivative of D with respect to k. The substitution of equations (5)-(7) leads to the displacement field u on the upper surface of the plate ($z = d$). The strain distribution can be obtained by the derivative $\varepsilon_x = \partial u/\partial x$:

$$u = i\sum_{k^S}\frac{\tilde{\tau}_{xz}^S}{D^{S'}}(N_{11}^S + 2d^2N_{14}^S + d^4N_{44}^S)e^{ik^Sx} + i\sum_{k^A}\frac{\tilde{\tau}_{xz}^A}{D^{A'}}(d^2N_{22}^A + 2d^4N_{25}^A + d^6N_{55}^A)e^{ik^Ax} \tag{13}$$

$$\varepsilon_x = -\sum_{k^S}\frac{k^S\tilde{\tau}_{xz}^S}{D^{S'}}(N_{11}^S + 2d^2N_{14}^S + d^4N_{44}^S)e^{ik^Sx} - \sum_{k^A}\frac{k^A\tilde{\tau}_{xz}^A}{D^{A'}}(d^2N_{22}^A + 2d^4N_{25}^A + d^6N_{55}^A)e^{ik^Ax} \tag{14}$$

The formulation of the shear stress τ_{xz}, which consider the shear-lag in the bonding layer, can be taken from [8]. This formulation can be extended for the case of interdigital transducers:

$$\tau_{xz}(x) = (-1)^n \, W_n \, \tau_0 a \left[-\Gamma \frac{\sinh(\Gamma[x - ns])}{\cosh(\Gamma a)} \right], \qquad n = 0, \dots, N_a - 1 \tag{15}$$

The Fourier transformation into the wavenumber domain is:

$$\tilde{\tau}_{xz}(k) = 2i \, \tau_0 a \, \Gamma \, \frac{\Gamma \sin(ka) - \mathrm{k} \tanh(\Gamma a) \cos(ka)}{\Gamma^2 + k^2} \sum_{n=0}^{N_a\text{-}1} (-1)^n \, W_n \, e^{-inks} \tag{16}$$

where N_a is the number of actuator segments, $2a$ the length of each segment, s the segment distance and W_n the apodization function. With an apodization each segment can be driven with different amplitudes, so that the frequency response function of the transducer is modified and the mode selectivity can be enhanced. As shown in Figure 2, adjacent transducer segments are driven with opposite polarity, which takes the term (-1) into account.

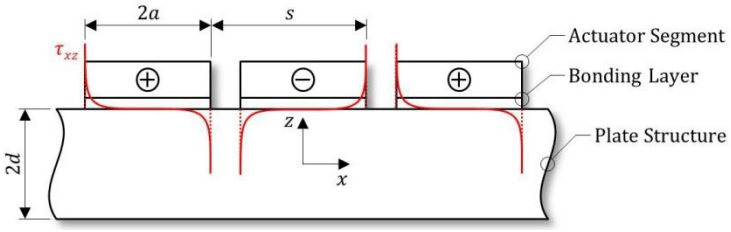

Figure 2 : Shear stress in the bonding layer

The force of the transducer $\tau_0 a$ and the shear-lag parameter Γ are given by [8]:

$$\tau_0 a = \left(\frac{\Psi}{\Lambda + \Psi} \right) t_a E_a d_{31} \frac{U}{t_a}, \quad \Gamma^2 = \frac{\mathrm{G_k}}{\mathrm{E_a}} \frac{1}{\mathrm{t_a t_k}} \left(\frac{\Lambda + \Psi}{\Psi} \right), \quad \Psi = \frac{2 d E_p}{t_a E_a} \tag{17}$$

with E_p, $2d$ and E_a, t_a as Young's moduli and thicknesses of the plate structure and the actuator, G_k and t_k as shear modulus and thickness of the bonding layer, V and d_{31} as applied electrical voltage and piezoelectric constant. The value Λ is varying between different Lamb wave modes and depends on the frequency. For the fundamental modes (S_0 and A_0) and low frequencies the value Λ can be approximated with $\Lambda = 4$ [9]. On the sensor side the mechanical strains are converted into electrical voltage. According to [5], the voltage of each sensor segment can be calculated for the two-dimensional case in the form:

$$U_n = \frac{d_{31} t_s E_s}{\bar{\varepsilon}_{33}^{\sigma} 2a(1 - \nu_s)} \int_{-a}^{a} \varepsilon_{x,s} \, dx \tag{18}$$

where E_s, t_s, ν_s are Young's modulus, thickness and Poisson ratio of the sensor, $\bar{\boldsymbol{\varepsilon}}^{\sigma}$ the dielectric permittivity and $\varepsilon_{x,s}$ the sensor strain. For interdigital transducer with N_s segments this formulation becomes:

$$U = \frac{d_{31} t_s E_s}{\bar{\varepsilon}_{33}^{\sigma} 2a(1 - \nu_s)} \sum_{n=0}^{N_s\text{-}1} (-1)^n \, W_n \int_{ns-a}^{ns+a} \varepsilon_{x,s} \, dx \tag{19}$$

To consider the shear-lag in the bonding layer on the sensor side, the strain distribution between the plate structure and the sensor is given as follows [8]:

$$\varepsilon_{x,s} = \varepsilon_{x,p} \left[1 - \frac{\cosh(\Gamma[x - ns])}{\cosh(\Gamma a)} \right], \qquad n = 0, \dots, N_s - 1 \tag{20}$$

Substitution of equation (20) into (19) yields:

$$U = \frac{d_{31} t_s E_s}{\bar{\varepsilon}_{33}^{\sigma} a(1-\nu)} \left[\begin{array}{l} -\sum_{k^S} \left[\frac{\sin(k^S a)}{k^S} - \frac{k^S \sin(k^S a) + \Gamma \tanh(\Gamma a)\cos(k^S a)}{\Gamma^2 + (k^S)^2} \right] C^S e^{ik^S x} \sum_{n=0}^{N_s\text{-}1} (\text{-}1)^n W_n \, e^{ink^S s} - \\ -\sum_{k^A} \left[\frac{\sin(k^A a)}{k^A} - \frac{k^A \sin(k^A a) + \Gamma \tanh(\Gamma a)\cos(k^A a)}{\Gamma^2 + (k^A)^2} \right] C^A e^{ik^A x} \sum_{n=0}^{N_s\text{-}1} (\text{-}1)^n W_n \, e^{ink^A s} \end{array} \right] \quad (21)$$

where:

$$C^S = \frac{k^S \tilde{\tau}_{xz}^S}{D^{S'}} \left(N_{11}^S + 2d^2 N_{14}^S + d^4 N_{44}^S \right), \quad C^A = \frac{k^A \tilde{\tau}_{xz}^A}{D^{A'}} \left(d^2 N_{22}^A + 2d^4 N_{25}^A + d^6 N_{55}^A \right) \quad (22)$$

The sensor voltage consists of solution for symmetric and anti-symmetric modes, which have to be individual determined by the wavenumbers k_s and k_a. The wavenumbers $k = k^{Re}\text{-}ik^{Im}$ are complex values in order to describe the dispersion as well as the attenuation characteristics of the plate structure. Accordingly, the phase velocities are determined by the real part $c_p = \omega / k^{Re}$ and the attenuation factors by the imaginary part k^{Im} of the wave numbers The complex wavenumbers can be examined in such a way that the equation of motion (1) is solved without the mechanical stresses of the actuator. The substitution of equation (8) and (3) and solving the equation of motion (1), where the stresses are equal to zero ($\tilde{\boldsymbol{\sigma}} = 0$), leads to an eigenvalue problem in the following form:

$$\boldsymbol{L}\hat{\boldsymbol{u}}_0 = 0 \quad (23)$$

The eigenvalue problem needs to be numerically examined. The method as well as the coefficients L_{ij} is detailed described in [6] and [7].

As excitation signal a sinus burst is used. The frequency spectrum of a sinus burst is given by [9]:

$$X_{Sign}(f) = \frac{n_p}{4f_0} \left[\operatorname{sinc}\left(\frac{\pi n_p}{2f_0} [f - f_0] \right) + (-1)^{n_p+1} \operatorname{sinc}\left(\frac{\pi n_p}{2f_0} [f + f_0] \right) \right] \quad (24)$$

The bandwidth $B_n = 4f_0/n_p$ can be calculated using the number of pulses n_p and the centre frequency f_0. To consider the frequency spectrum of the excitation signal X_{Sign} within the sensor signal U_{Mono} of equation (21) the following formulation is utilized:

$$U_{Band}(f_0) = \sum_{n=f_0 - B_n/2}^{f_0 + B_n/2} U_{Mono}(n) \cdot X_{Sign}(n) \cdot \Delta f \quad (25)$$

where Δf describe the discrete frequency increments. In equation (25) only the main lope in the frequency spectrum of the excitation signal, which has the bandwidth B_n, is taken into account. The last step is to transform the spectral sensor signals from the frequency-space domain into the time-space domain. This can be done by an inverse Fourier transformation, which cannot be calculated analytically. Therefore a discrete Fourier transformation, especially a fast Fourier transform algorithm has to be used.

2 RESULTS

For the implementation of the model algorithms the commercial software *MATLAB*® is used. The investigations on are carried out on a quasi-isotropic CFRP plate. This plate consist of 7 plies in a $[(0/90)_{360}/+45/\text{-}45/(\overline{0/90})_{220}]_S$ configuration. The mechanical properties of each ply are shown in the appendix. For the transducers the piezoceramic material *PIC255* (*PI Ceramic GmbH*) is chosen [11]. The bonding layer is made from an epoxy adhesive which exhibits a shear modulus of $G_k = 0.4$ GPa. The transducers are applied in 0°-direction ($\theta_p = 0$) on the upper surface of the plate. The distance between actuator and sensor is set to $l = 200$ mm. All further parameters are summarized in the following Table 1.

s [mm]	$2a$ [mm]	N_a [-]	N_s [-]	t_a, t_s [mm]	t_k [µm]	G_k [GPa]	l [mm]	θ_p [°]	n_p [-]	B_n [-]
5	$0.8 \cdot s$	10	1	0.2	50	0.4	200	0	10	$4/n_p$

Table 1: Standard parameters of the analytical model

The Figure 3 shows the sensor voltage over frequency for an unapodized actuator and an apodized actuator which is weighted with the Blackman-Nuttall function.

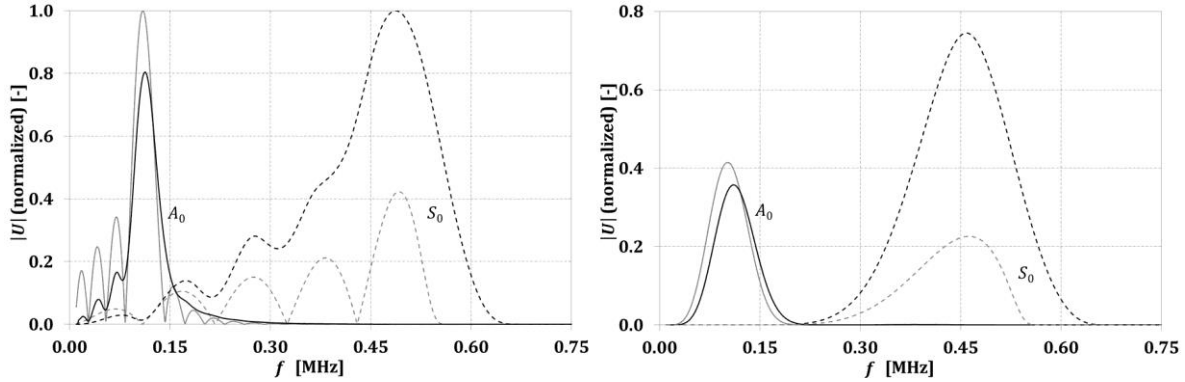

Figure 3 : Sensor voltage without apodization (left) and with apodization (right), black: spectral excitation signal, grey: mono-frequent excitation signal

The frequency response function is characterized by main and side lopes. The maximums of the main lopes occur when the segment distance correspond to the wavelength of the desired mode:

$$s = (2n-1)\frac{\lambda}{2}, \quad n = 1,2,3 \ldots \tag{26}$$

The maximum of the A_0 mode can be observed at 109 kHz, whereas the maximum of the S_0 mode is at 487 kHz. Due to the bandwidth of the spectral excitation signal the maximums and minimums are varying. With increasing frequency the signal bandwidth grows and therefore the amplitudes rise. Regarding the mode selectivity it is important that the main lope of the desired mode correspond to a minimum within the side lopes of the undesired mode. If this is the case, the mode selectivity is maximized. The location of the side lopes as well as their minimums can be controlled by the number of segments. The amplitudes of the side lopes can also be reduce by applying an apodization function to the transducer. Investigations on the model have shown that an apodization with the Blachman-Nuttall function produces the best results. As shown in Figure 3 (right) the amplitudes of the side lopes can be sufficient reduced. But on the other hand the bandwidth of the main lope increases due to the apodization. The following Figure 4 shows the sensor signal for different actuator configurations regarding number of segments and apodization.

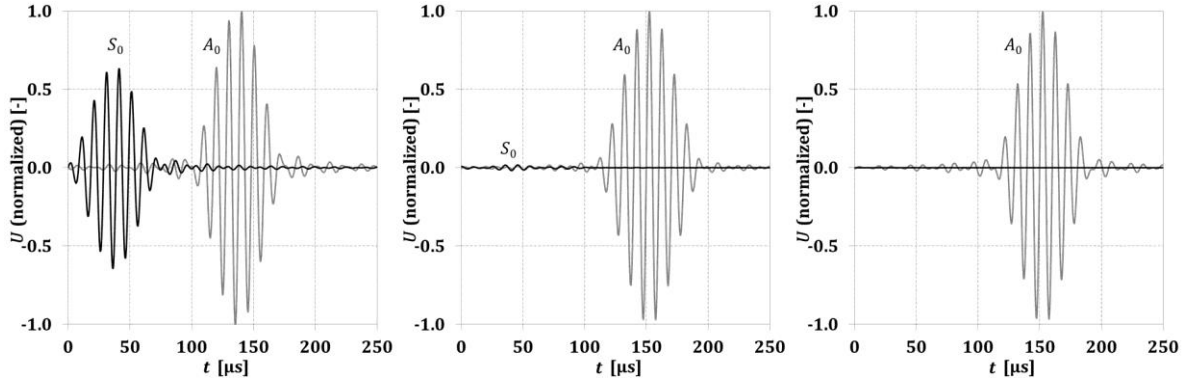

Figure 4 : Sensor signal at a centre frequency of f = 109 kHz, left: unapodized actuator (N_a = 1), centre: unapodized actuator (N_a = 10), right: apodized actuator (N_a = 10)

A centre frequency of 109 kHz is chosen at which the A_0 mode shows a maximum in its frequency response function. The sensor signals are normalized to the maximum of the A_0 mode ($U = 1$). It can be seen that the amplitude of the S_0 mode can be reduces from 0.63 to 0.017 when the number of segments will be increased from 1 to 10. But in this case the S_0 mode is still observable in the sensor signal. If an apodization is applied to the transducer the S_0 mode is not anymore observable in the signal because its amplitude is reduces to $2.18 \cdot 10^{-5}$.

CONCLUSION

In this paper a method of modelling the propagation of Lamb wave modes between actuators and sensors in composite plate is presented. A two dimensional analytical model is developed which is based on higher order laminated plate theory. The actuators and sensors are realized within the modelling in form of interdigital transducers. This kind of transducer is able to excite a particular Lamb wave mode and as a result to reduce the complexity of multimodal Lamb wave field. The results of the analytical model show that mode selective excitation and receiving of S_0 or A_0 mode can be achieved by interdigital transducers.

APPENDIX

The coefficients L_{ij} for symmetric modes of equation (10) are given by:

$$L_{11}^S = A_{11}k_x^2 + 2A_{16}k_xk_y + A_{66}k_y^2 - \omega^2 I_0\,, \qquad L_{13}^S = -i\kappa_3\left[A_{13}k_x + A_{36}k_y\right]$$

$$L_{14}^S = D_{11}k_x^2 + 2D_{16}k_xk_y + D_{66}k_y^2 - \omega^2 I_2\,,$$

$$L_{33}^S = -\left[\kappa_4^2 D_{55}k_x^2 + 2\kappa_4\kappa_5 D_{45}k_xk_y + \kappa_5^2 D_{44}k_y^2 + \kappa_3^2 A_{33} - \omega^2 I_2\right]$$

$$L_{34}^S = -i[\kappa_3 D_{13} - 2\kappa_4^2 D_{55}]k_x - i[\kappa_3 D_{36} - 2\kappa_4\kappa_5 D_{45}]k_y$$

$$L_{44}^S = H_{11}k_x^2 + 2H_{16}k_xk_y + H_{66}k_y^2 + 4\kappa_4^2 D_{55} - \omega^2 I_4$$

The coefficients L_{ij} for anti-symmetric modes of equation (10) are given by:

$$L_{11}^A = -\left[\kappa_1^2 A_{55}k_x^2 + 2\kappa_1\kappa_2 A_{45}k_xk_y + \kappa_2^2 A_{44}k_y^2 - \omega^2 I_0\right], \quad L_{12}^A = i\kappa_1\left[\kappa_1 A_{55}k_x + \kappa_2 A_{45}k_y\right]$$

$$L_{14}^A = -\left[\kappa_1\kappa_7 D_{55}k_x^2 + (\kappa_2\kappa_7 + \kappa_1\kappa_8)D_{45}k_xk_y + \kappa_2\kappa_8 D_{44}k_y^2 - \omega^2 I_2\right]$$

$$L_{15}^A = 3i\left[\kappa_1\kappa_7 D_{55}k_x + \kappa_2\kappa_7 D_{45}k_y\right], \qquad L_{22}^A = D_{11}k_x^2 + 2D_{16}k_xk_y + D_{66}k_y^2 + \kappa_1^2 A_{55} - \omega^2 I_2$$

$$L_{24}^A = i\left[\kappa_1\kappa_7 D_{55}k_x - 2\kappa_6\left(D_{13}k_x + D_{36}k_y\right) + \kappa_1\kappa_8 D_{45}k_y\right]$$

$$L_{25}^A = H_{11}k_x^2 + 2H_{16}k_xk_y + H_{66}k_y^2 + 3\kappa_1\kappa_7 D_{55} - \omega^2 I_4$$

$$L_{44}^A = -\left[\kappa_7^2 H_{55}k_x^2 + 2\kappa_7\kappa_8 H_{45}k_xk_y + \kappa_8^2 H_{44}k_y^2 - 4\kappa_6^2 D_{33} - \omega^2 I_4\right]$$

$$L_{45}^A = 3i\left[\kappa_7^2 H_{55}k_x + \kappa_7\kappa_8 H_{45}k_y\right] - 2i\kappa_6\left[H_{13}k_x + H_{36}k_y\right]$$

$$L_{55}^A = K_{11}k_x^2 + 2K_{16}k_xk_y + K_{66}k_y^2 + 9\kappa_7^2 H_{55} - \omega^2 I_6$$

The stiffness coefficients and mass moment of inertia can be calculated as follows:

$$\left(A_{ij}, B_{ij}, D_{ij}, F_{ij}, H_{ij}, J_{ij}, K_{ij}\right) = \sum_{n=1}^{N_L} \int_{z_{n-1}}^{z_n} C_{ij,n} \cdot (1, z, z^2, z^3, z^4, z^5, z^6)\,dz$$

$$(I_0, I_1, I_2, I_3, I_4, I_5, I_6) = \sum_{n=1}^{N_L} \int_{z_{n-1}}^{z_n} \rho_n \cdot (1, z, z^2, z^3, z^4, z^5, z^6)\,dz$$

where N_L are the number of laminate plies, $C_{ij,n}$ the stiffness matrix and ρ_n the density of the n-th laminate ply. In case of symmetric laminates the coefficients B_{ij}, F_{ij} and J_{ij} as well as I_1, I_3 and I_5 are equal to zero. Within experimental investigation, presented in [7], the shear correction factors are chosen as $\kappa_1 = \kappa_2 = \kappa_4 = \kappa_7 = \kappa_8 = \pi^2/\sqrt{11}$, $\kappa_3 = \pi^2/\sqrt{12}$ and $\kappa_5 = \kappa_6 = \pi^2/\sqrt{15}$. The following Tables 2 and 3 show the elastic and viscoelastic material properties of each ply of the CFRP plate, which are determined within experimental investigations [7].

Ply	t [mm]	ρ [kg/m³]	C_{11}^{Re} [GPa]	C_{12}^{Re} [GPa]	C_{13}^{Re} [GPa]	C_{22}^{Re} [GPa]	C_{23}^{Re} [GPa]	C_{33}^{Re} [GPa]	C_{44}^{Re} [GPa]	C_{55}^{Re} [GPa]	C_{66}^{Re} [GPa]
$(0/90)_{220}$	0.20	1560	53.81	2.21	1.86	54.32	2.80	8.59	2.87	2.87	3.83
$(0/90)_{360}$	0.40	1520	50.08	2.09	1.81	50.58	2.73	8.32	2.67	2.67	3.56
$(45)_{250}$	0.25	1550	129.28	3.36	3.36	9.08	3.22	9.08	2.93	5.58	5.58

Table 2: Ply thickness t, density ρ and elastic material properties of the laminate plies

Ply	η_{11} [GPa]	η_{12} [GPa]	η_{13} [GPa]	η_{22} [GPa]	η_{23} [GPa]	η_{33} [GPa]	η_{44} [GPa]	η_{55} [GPa]	η_{66} [GPa]
$(0/90)_{220}$	1.10	0.04	0.03	1.00	0.004	0.01	0.03	0.05	0.10
$(0/90)_{360}$	1.10	0.04	0.03	1.00	0.004	0.01	0.06	0.03	0.10
$(45)_{250}$	2.00	0.05	0.05	0.90	0.84	0.90	0.03	0.25	0.25

Table 3: Viscoelastic material properties of the laminate plies

REFERENCES

[1] Veidt, M., Liu, T., Kitipornchai, S.: Modelling of Lamb waves in composite laminated plates excited by interdigital transducers, NDT&E International 35, 437-447, 2002

[2] Monkhouse, R. S. C., Wilcox, P. W., Lowe, M. J. S., Dalton, R. P., Cawley, P.: The rapid monitoring of structures using interdigital Lamb wave transducers, Smart Materials and Structures 9, pp. 304–309, 2000

[3] Monkhouse, R. S. C., Wilcox, P. D., Cawley, P: Flexible interdigital PVDF transducers for the generation of Lamb waves in structures, Ultrasonics 35, 489–498, 1997

[4] Wang, L.: Elastic Wave Propagation in Composites and Least-Squares Damage Localization Technique, North Carolina State University, PhD Thesis, 2004

[5] Calomfirescu, M.: Lamb Waves for Structural Health Monitoring in Viscoelastic Composite Materials, Science-Report Faserinstitut Bremen, University of Bremen, PhD Thesis, 2008

[6] Torres-Arredondo, M. A., Fritzen, C. P.: A viscoelastic plate theory for the fast modelling of Lamb wave solutions in NDT/SHM applications, Ultragarsas (Ultrasound), vol. 66 (2), pp. 7-13, 2011

[7] Schmidt, D., Sadri, H., Szewieczek, A., Sinapius, M., Wierach, P., Siegert, I., Wendemuth, A.: Characterization of Lamb wave attenuation mechanisms, SPIE-Smart Structures/NDE, Proceedings, 8695-2, San Diego, USA, 2013

[8] Giurgiutiu, V.: Structural Health Monitoring with Piezoelectric Wafer Active Sensors, Academic Press - Elsevier, 2008

[9] Yu, L. , Bottai-Santoni, G., Giurgiutiu, V.: Shear lag solution for tuning ultrasonic piezoelectric wafer active sensors with applications to Lamb wave array imaging, International Journal of Engineering Science, vol. 48, no. 10, pp. 848-861, 2010.

[10] Raghavan, A.: Guided-Wave Structural Health Monitoring, University of Michigan, PhD Thesis, 2007.

[11] PI Ceramic GmbH: Piezoelectric Ceramic Products – Fundamentals, Characteristics and Applications, 2011